Positron annihilation spectroscopy investigation of defects in neutron irradiated tungsten materials

V. Chatzikos[1,2], K. Mergia[1,*], G. Bonny[3], D. Terentyev[3], D. Papadakis[1], G.E. Pavlou[1], and S. Messoloras[1]

[1] National Centre for Scientific Research "Demokritos", Institute of Nuclear and Radiological Science and Technology, Energy and Safety, 15341 Agia Paraskevi, Athens, Greece

[2] Department of Physics, School of Sciences, University of Ioannina, Ioannina, 45110, Greece

[3] SCK CEN, Nuclear Materials Science Institute, Boeretang 200, B-2400 Mol, Belgium

Abstract

The identification of defects in neutron damaged materials is essential for elucidating the correlation between the microstructure and the properties of a material. Positron annihilation spectroscopy (PAS) is very sensitive in open volume defects and thus a useful tool for the investigation of the radiation damage in matter. Tungsten is a critical material for the first wall and divertor of fusion reactors. In the current work, the evolution of the open volume defects in tungsten (W) materials neutron irradiated to 0.12 displacements per atom (dpa) and in the temperature range from 600 to 1200 °C in the Belgian Material Test Reactor BR2 is investigated by positron annihilation lifetime and coincidence Doppler broadening spectroscopy. Three tungsten grades were studied: W(100) single crystal, ITER grade forger bar and heavily deformed "cold"-rolled sheet. PAS results show that the neutron irradiation results in the formation of dislocations and voids of size larger 1 nm at all irradiation temperatures and in all W grades. The dislocation and void density decreases with increasing irradiation temperature. Moreover, the void size increases with the increase of the irradiation temperature.

1 Introduction

Tungsten (W) and its alloys are promising armor materials for the divertor and the first wall in fusion reactors due to their attractive properties such as high melting point, high thermal conductivity, low tritium retention, low swelling under irradiation and resistance in sputtering, thermal stresses and shock [1, 2]. However, W is brittle at low temperatures and the ductile to brittle transition temperature (DBTT) ranges from room temperature to several hundred degrees Celsius [1]. In addition, tungsten plasma facing components will be subject to high energy (up to 14 MeV) neutron irradiation, high heat fluxes in the range 10-20 MW/m^2 and

* Corresponding author: Konstantina Mergia, kmergia@ipta.demokritos.gr

energetic impinging particles from the plasma [3]. The understanding of the effects of each of these extreme conditions on the properties of W is crucial for the development of structural modifications that will warrant the safe and prolonged life of W plasma facing components. Within the framework of the EUROfusion project WPMAT [4], neutron irradiations of different W material microstructures at different doses and in the temperature range from 600 to 1200 ºC have been carried out. One of the aims of this work was to advance the understanding of the basic phenomena connected with the neutron irradiation on tungsten.

In the literature, there is a number of investigations regarding the microstructure evolution and mechanical properties of tungsten and its alloys under fission neutron irradiation [5, 6, 7, 8, 9, 10, 11, 12, 13, 14, 15, 16, 17, 18, 19, 20, 21, 22, 23, 24, 25, 26, 27]. Neutron irradiation results in the formation of point defects that diffuse and cluster to form voids and dislocation loops. In addition, transmutation reactions result in the production of Re, Os and Ta which diffuse and form clusters or precipitates. These three types of defects, i.e. voids, dislocation loops and transmutation product clusters, cause increase in hardness and yield strength and decrease in ductility [23,24,26]. Dislocation loops prevail at irradiation temperatures below 500 °C, while the increase of the irradiation temperature and dose promote void formation and precipitates (for doses larger than about 1 dpa) [6, 12]. Formation of a lattice of voids with a lattice parameter of 19.5 nm has been observed after irradiation at 550 °C to a fast neutron fluence of 10^{22} n/cm^2 [28]. Moreover, it has been shown that hardness and microstructure changes exhibit a clear dependence on the neutron energy spectrum [11]. In [12], irradiation hardening in the range 34–52% was observed in single crystal tungsten presenting a maximum at 800 °C. The peak hardening was linked to the peak density of voids and it was shown that voids are the main contribution of the irradiation hardening. In [22], neutron irradiation of W single crystal was performed in the temperature range 600 - 1200 °C to a dose of 0.12 displacements per atom (dpa) and the maximum hardening was observed at the irradiation temperature of 600 °C, corresponding to a maximum defect density of about 8×10^{23} m^{-3} with the latter showing a three-fold decrease after irradiation at 1200 °C. In neutron irradiated polycrystalline W, to a dose of about 0.2 dpa and in the temperature range 600 – 1200 °C, voids and dislocation loops were observed after neutron irradiation in the temperature range 600 - 1200 °C, with their number density decreasing and their size increasing with the increase of the irradiation temperature [23, 24].

The development of W based radiation resistant material microstructures and the prediction of the behavior of the material parts of a component under neutron irradiation at fusion relevant conditions is of major importance in the fusion roadmap. The aim of the present study is to contribute to the fundamental understanding of neutron irradiation effects in tungsten and to complement the insight in the evolution of open volume defects in neutron irradiated materials of different microstructures as a function of the irradiation temperature. To this end, positron annihilation lifetime and coincidence Doppler broadening spectroscopy were

employed as being sensitive tools in the determination and the characterization of the open volume defects. The annihilation characteristics, namely the positron lifetime and its associated intensity, as well as, the momentum distribution of annihilation photons in the material provide information about the type of the open volume defects, the defect population and the surrounding chemical environment at the annihilation site. The effect of the initial microstructure on the generated open volume defects is examined by investigating both single crystal and deformed polycrystalline tungsten materials with different degrees of plastic deformation.

2 Experimental Details

2.1 Material and irradiations

Three types of W materials are investigated: a) Single crystal W(100) of 99.999 % purity having a diameter of 12 mm and supplied by MaTeck, b) W cold rolled sheet of 1 mm thickness, and c) W bar forged by hammering from two orthogonal sides. The W sheet [29] and bar [30] materials were produced by PLANSEE SE in sheet and bar form, respectively, using a powder metallurgical route consisting of sintering and rolling or forging. The sheet sintered compact was heated to a temperature of above 1250 °C and subsequently rolled to a thickness of 5.5 mm ("hot"-rolling). Then this sheet is "cold"-rolled to a temperature of below 1000 °C and it is brought by progressive rolling steps to a thickness of 1 mm. The microstructure of the resulting material consists of plate-like grain shapes and the grains are elongated along the rolling direction (Fig.1) [31]. The bar material has a square cross-section of 36 mm × 36 mm and due to its hammering from two orthogonal directions, the grains are needle-like and are elongated along the bar axis (Fig.1) [30, 31].

Disks with thickness of 1 mm were sectioned using electrical discharge machining and were subsequently mechanically polished from both sides using diamond suspension for removing the surface oxide and stresses/surface damage induced by the EDM cutting. At the final stage colloidal silica was used in order to obtain mirror quality surface. The resulting thickness of the samples was about 0.5 mm.

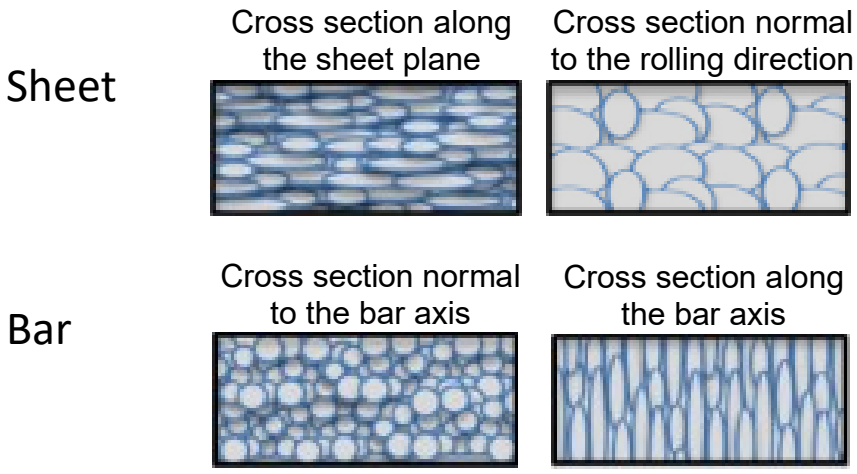

Fig. 1. Schematic grain structure of the W polycrystalline materials.

Neutron irradiations were performed in the Belgian Material Test Reactor (BR2). The samples were encapsulated in 1.5 mm stainless steel tube filled with helium. In order to maximize the fast-to-thermal neutron ratio and thus achieve transmutation rates of W into Re and Os as close as possible to those expected in ITER and DEMO conditions, the irradiation was performed inside the fuel element in the maximum fast neutron (> 0.1 MeV, 7×10^{14} n/cm^2/s) flux position and the thickness of the steel tube was adjusted to maximize the shielding from the thermal neutrons.

The gap between the encapsulating stainless steel tube and the samples was adjusted, based on thermal and neutronic calculations, to achieve the irradiation temperatures of 600, 800, 900 and 1200 °C. The irradiation dose was 0.12 displacement per atom (dpa); it was calculated by MCNPX 2.7.0 based on the total fast neutron fluence (5.8×10^{20} n/cm^2, >0.1 MeV) and was reached after two reactor cycles of a total duration of 49 days [32]. For the dpa calculations the cross sections for W have been prepared from the JENDL4 file (MT444) for the threshold displacement energy of 55 eV according to the IAEA recommendation of [33]. For the calculation of the transmutation of W to Re, Os and Ta FISPACT-II and TENDL-2019 (for Re and Os) and EAF-2010 (for Ta) cross section libraries were used and were found in the range of 0.38-0.43 at% Re, $(6.2\text{-}7.8)\times10^{-3}$ at% Os and $(1.5\text{-}1.7)\times10^{-3}$ at% Ta. The use of the nuclear libraries was based on gamma spectroscopy validation measurements of the calculated versus experimental specific activities (to be published).

2.2 Microstructure

TEM measurements were performed on the unirradiated materials with JEOL 3010 electron microscope operating at 300 kV. The details of the measurements can be found in [31].

2.3 Positron annihilation spectroscopy

2.3.1 Positron annihilation lifetime spectroscopy (PALS)

Positron annihilation lifetime spectroscopy (PALS) is a powerful and sensitive method for the investigation of open volume defects with concentrations as low as 10^{-6} in materials [34, 35]. The positron, when implanted in a material, is very fast thermalized (~10^{-12} s), it gets trapped within open volume defects and finally annihilates with an electron producing two gammas. The positron lifetime is inversely proportional to the electron density around the positron position. The reduced electron density at an open volume defect site, such as a vacancy, divacancy, dislocation or vacancy cluster, delays positron annihilation and, thus, increases the positron lifetime. The positron lifetime increases as the size of the open volume defect increases. The effective positron lifetime in the delocalized state varies inversely proportional with the sum of the positron annihilation rate and the trapping rate. The trapping rate depends on the types of defects in the sample and is proportional to the defect concentration. It should be mentioned that grain boundaries (GBs) should not affect positron trapping since the grain size of the polycrystalline materials in the current study is of the order of a few micrometers [31] and only in the nano-crystalline materials positron trapping may take place at GBs.

The principle of operation of the lifetime spectrometer is to measure the number of events for different time intervals from the positron generation to its annihilation. The positron generation, start signal, is signaled by the prompt gamma rays (E=1.274 MeV) following the emission of positrons and positron annihilation, stop signal, is indicated from the annihilation gamma photons (E=0.511 MeV). Positron annihilation lifetime measurements were carried out at room temperature using Ortec® PLS-system. As the positron source the ^{22}Na radionuclide (from evaporated ^{22}NaCl metallic salt), and with a half-life of 959.8 days has been used. The positron source, with an activity of 100 μCi, is encapsulated in 7.5 mg/cm^2 thin polymide (Kapton®) windows and has an active area of 5 mm. For the measurements the positron source is sandwiched between two pieces of identical specimens. The gamma rays are detected using fast plastic scintillators coupled with photomultiplier (PM) tubes placed at a distance of 3 mm from the sample. The time resolution, i.e. the Full Width Half Maximum (FWHM) of the prompt spectrum, was measured with ^{60}Co and was found around 270 ps. For each spectrum at least four million counts were collected.

The maximum penetration in tungsten of the positrons emitted by ^{22}Na (545 keV maximum energy) is around 50 μm, which is lower than the samples thickness, i.e. all positrons are annihilated within the sample. The mean penetration depth of positrons having the mean energy of the ^{22}Na spectrum, i.e. 215 keV, is 11 μm, which is large enough to avoid any surface effects. On the other hand the two 0.511 MeV gammas emitted during the positron annihilation events have very small absorbance (~10%) by the tungsten material.

The data analysis was performed using LT10 software [36, 37]. The experimental spectra were fitted to the expression [36],

$$S(t) = B + R(t) \otimes \left(I_{src} + I_s \right) = B + R(t) \otimes \left(\sum_{k=1}^{L} I_k \lambda_k e^{-\lambda_k t} + \sum_{i=0}^{N} I_i \lambda_i e^{-\lambda_i t} \right) \quad (1)$$

which involves a sum of exponential components referring to the source, I_{src}, and to sample, I_s, convoluted by the resolution function $R(t)$ (assumed Gaussian) and the background B. The defect free material is referred as $i = 0$ and $i = 1,...,N$ corresponds to the different open volume defects of the sample. Each component is characterized by two parameters: the intensity I_i and the lifetime $\tau_i = 1/\lambda_i$. The components k refer to air, kapton and source part of the spectrum . In this expression it is assumed that in each defect the positron is annihilated independently of the other defects and the defect free matrix, i.e. there are no correlations.

Since positrons may annihilate both in the source materials (^{22}NaCl) and the thin foil encapsulating it, and these processes contribute additional lifetime components to the PALS spectrum it is essential to determine these components in order to obtain reliable values of the lifetimes and intensities of the W investigated samples. To this end, a number of reference well annealed materials (Al, Ni, Cd and Pb) of high purity (better than 99.99%) were analyzed in order to determine the source parameters. Two source components were considered; one for the annihilations in the ^{22}Na source and Kapton® foil (because of their very similar lifetimes) and another one for the annihilations in the air between the source and the specimen. The contribution of those components to the spectrum depends on the atomic number of the sample surrounding the source and this was found equal to 53% for tungsten.

The obtained lifetimes of the reference materials were found in very good agreement with the values reported in the literature. The lifetime value of the first source component, $\tau_{src,1}$, comprising the annihilations in the source itself and the surrounding Kapton® foil was found (375 ± 1) ps and it is in good agreement with values reported in the literature (in the range 368 - 386 ps for Kapton and NaCl source in [37, 38, 39], 385 ps for Kapton in [40]). The second source component, $\tau_{src,2}$, corresponding to the annihilations in the air between the source and the specimen, exhibits a lifetime value of (2.56 ± 0.08) ns and relative intensity of

the source contribution I_{air} =(2.4 ± 0.4)%; similar values in the range 1.4 – 1.9 ns are reported in literature [37, 39, 41, 42].

2.3.2 Coincidence Doppler broadening positron annihilation spectroscopy (CDB-PAS)

Positron annihilation spectroscopy (PAS) was used to determine the coincidence Doppler broadening (CDB) spectrum in the irradiated samples. The CDB spectrum provides the momentum distribution of the electrons in the material. Low momentum is associated to valence/free electrons and high momentum is associated to core electrons, which can be used to determine the chemical environment around a positron–electron annihilation site. In case of positrons trapped at a defect site, the relative contribution from core electrons towards annihilation is drastically reduced as compared to valence electrons. As a result, there is an increase in the low momentum region (valence electron) and a concomitant decrease in high momentum region (core electrons). The contributions in low and high momentum regions of the annihilation peak are defined as S- and W-parameters.

The CDB setup [14,43,44] consists of two movable high-purity Ge detectors (coaxial HPGe detector from Canberra type GC3018) with high-energy resolution (FWHM = 0.8 keV at 122 keV and FWHM = 1.8 keV at 1332 keV) and built-in preamplifier (model 2101P). A digital signal processor (DSP Canberra Model 2060) for each detector and personal computer with LabView acquisition board card were used to collect the spectra. Both the electronics (two detectors and coincidence) as well as the hardware (biological shielding and mobility of the detectors) were optimized to measure highly active specimen with moderate detector dead time (< 20%) and very low background.

The measurements were performed at room temperature using a ^{22}Na positron source. The positron source was sandwiched between two identical samples, such that the fraction of positron annihilations outside the samples is negligible.

The S- and W-parameters were defined as the ratio of low momentum and high momentum regions in the CDB spectrum to the total region, respectively. Up to some extent, the limits enclosing S- and W-parameters are arbitrary, as long as they are well separated. For comparison with Hu et al. [http://dx.doi.org/10.1016/j.jnucmat.2015.12.040], we have taken the same limits: $|p_L| < 2.78 \times 10^{-3}\, m_0 c$ for the S-parameter and $7.28 \times 10^{-3}\, m_0 c < |p_L| < 29.12 \times 10^{-3}\, m_0 c$ for the W-parameter. Here c denotes the lightspeed, m_0 the electron rest mass and p_L the longitudinal component of the positron-electron momentum along the direction of the γ-ray emission.

3 Results

3.1 Microstructure of the reference materials

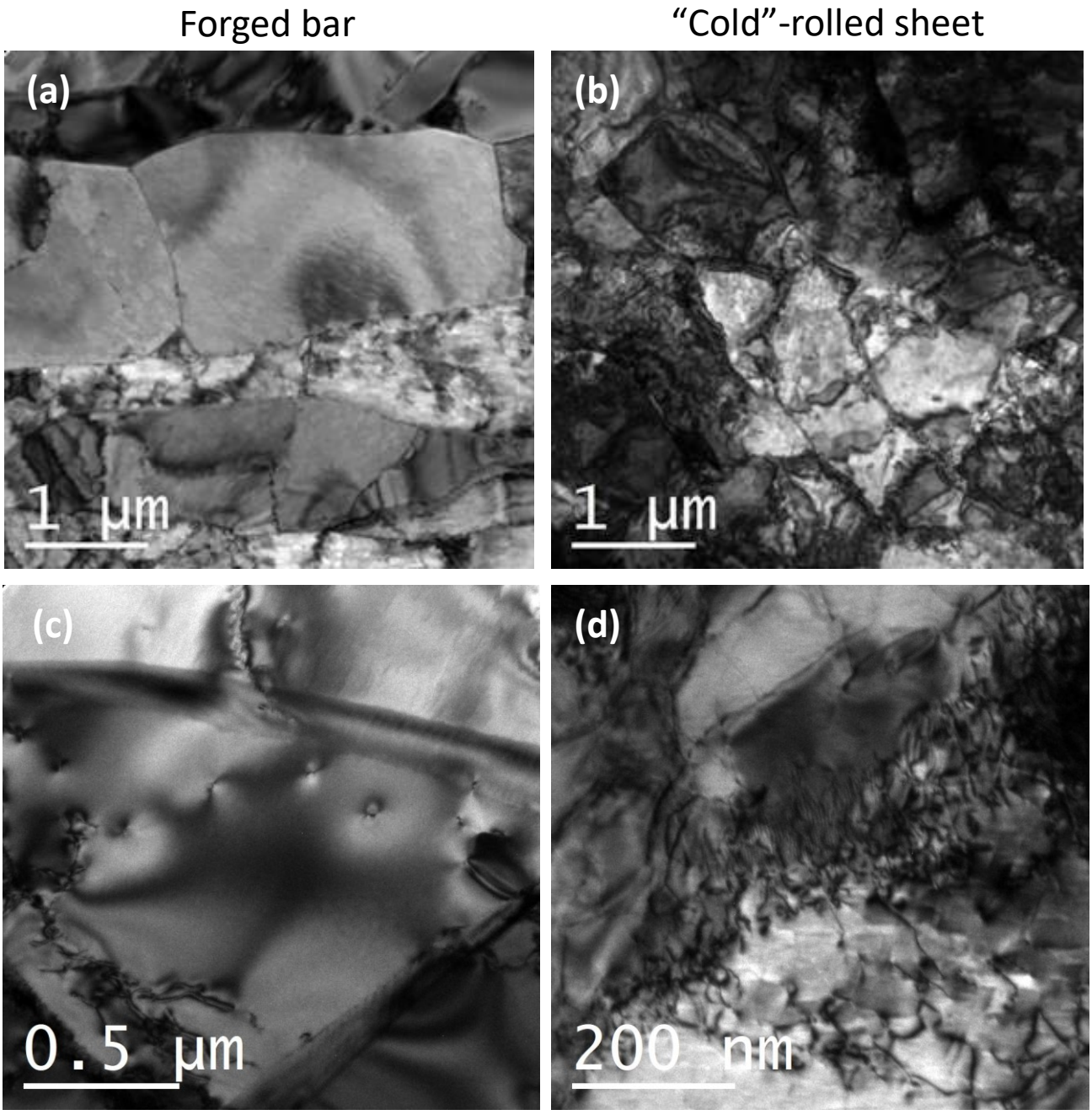

Fig. 2. TEM images of the reference microstructure of the W forged bar (a),(c) with the horizontal axis along the bar axis, and W “cold”-rolled sheet (b), (d).

The typical reference microstructure of the investigated polycrystalline W materials as determined by TEM measurements is presented in Fig.2 (for details see [23]). For the bar the sub-grains have elongated shape and their sizes vary in the range 0.6–1.7 μm in the normal to the bar axis and 2.3–4 μm along the bar axis (Fig. 1a). The dislocation density depends on the particular sub-grain, ranging from 4 to 8 × 10^{12} m^{-2}, and has an average value of 4.5 × 10^{12} m^{-2}. Most of the grain boundaries are low-angle type grain boundaries. For the W sheet the visible sub-grain size is in the range 1.5 – 2 μm, while it presents a dense tangled dislocation network with an average dislocation density of (9.8 ± 2.0)×10^{13} m^{-2} and low angle grain boundaries (Fig.2(b),(c)).

3.2 Characterization of open volume defects using PALS

The normalized PALS spectra of the unirradiated and irradiated samples are presented in Fig.3 for the four irradiation temperatures. The impact of neutron irradiation on the spectra is evident. As Fig.3 suggests, neutron irradiation on tungsten samples results in the increase of the average positron lifetime at all irradiation temperatures.

Below we initially discuss the results on the unirradiated samples and subsequently those of the irradiated ones.

3.2.1 Unirradiated materials

Equation (1) is used to analyze the PALS spectra of the unirradiated tungsten samples. For the SC one lifetime is needed to describe the spectra which is found to be (114 ± 1) ps, whereas for the bar and the sheet two lifetimes are required. The results are presented in Table 1. For the SC material the obtained lifetime is in agreement with the positron lifetime in defect-free W material reported in the literature in the range 100-116 ps [45, 46, 47, 48, 49, 50, 51]. This lifetime was used as fixed to describe the positron annihilation in the defect free part of the W polycrystalline materials and the second lifetime, τ_1, and its intensity were least square fitted.

Before discussing our results, we summarize the necessary relevant information for the interpretation obtained from the literature. The positron lifetimes for mono-vacancy and dislocation defects are reported in the range of 160-200 ps and 130–180 ps, respectively [47, 48, 52, 53, 54]. The low lifetime value of 130 ps corresponds to screw dislocations as calculated by Staikov et al [50]. Also, the positron lifetime of a vacancy associated to either screw or edge dislocation was calculated in the range 188-192 ps [50].

The forged bar and "cold"-rolled sheet materials present similar τ_1 values which correspond to positron annihilations in dislocations and vacancies associated or not with them. The "cold"-rolled material though presents a quite larger relative intensity, I_1, associated with the defects of about 77% compared to 45% for the bar. This indicates that the "cold"-rolling process causes the formation of a larger density of dislocations than the forging process. This observation is in good agreement with TEM results which show almost an order of magnitude larger dislocation density in the W sheet compared to that of the bar [31].

Table 1. Positron lifetimes and relative intensities obtained from least square fit of equation (1) to PALS spectra for the unirradiated samples. The dislocation density as determined by TEM is also presented.

	τ_0 (ps)	I_0 (%)	τ_1 (ps)	I_1 (%)	Dislocation density (m^{-2})
SC	114 ± 1	100%	-	-	-
Forged bar	114 (fixed)	55 ± 3	185 ± 8	45 ± 3	4.5×10^{12}
"Cold"-rolled sheet	114 (fixed)	25 ± 15	171 ± 17	75 ± 15	9.8×10^{13}

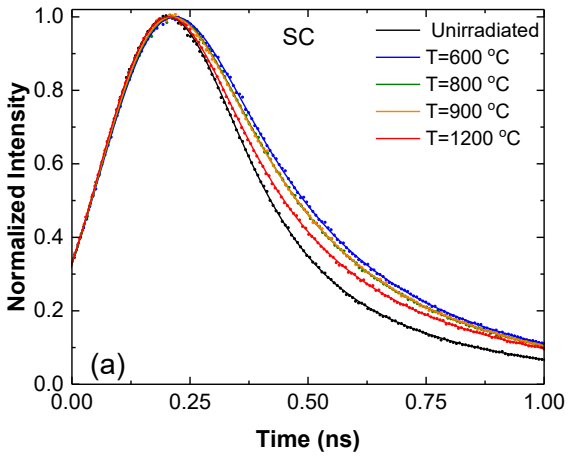

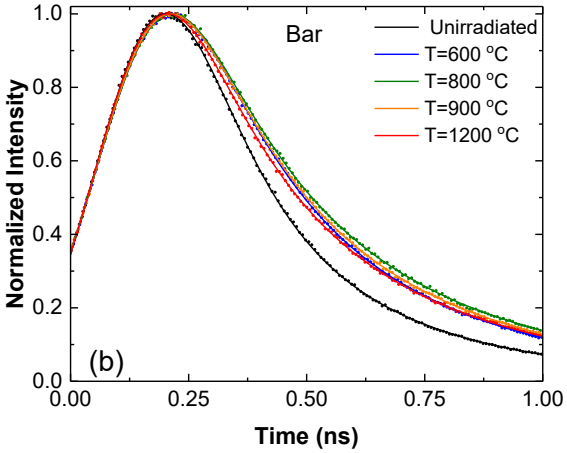

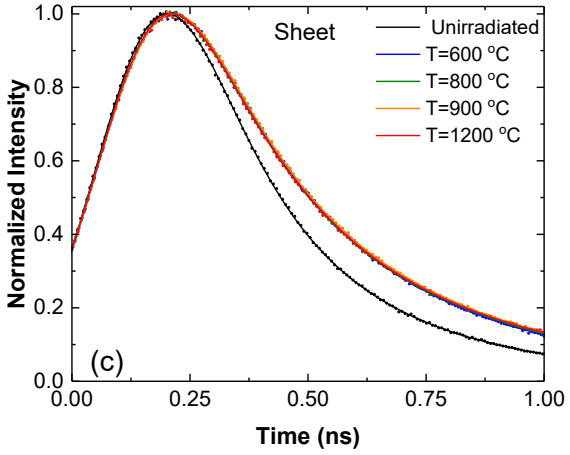

Fig.3. Normalized positron lifetime spectra for the unirradiated and irradiated W materials at various irradiation temperatures to a dose of 0.12 dpa. The solid lines are least-square fits of eq. (1) to the data. Zero time has been set arbitrarily.

3.2.2 Irradiated materials

Two lifetimes are required to describe the spectra of all the irradiated samples. The exponential model analysis is used to determine the lifetimes and their related intensities by least squares fitting of equation (1) to the spectra. In the following sections we present the PALS results for each material type. For the comparison with the unirradiated material the average lifetime of the latter is used, since as it will be explained below the average lifetime of the unirradiated materials corresponds to the same types of defects as those of the short lifetime of the irradiated materials.

a) Single crystal W(100)

The lifetimes and their related intensities, as determined by least squares fitting of eq. (1) to the data, together with the average lifetime, τ_{av}, are depicted in Fig. 4. The average positron lifetime provides a convenient single parameter description of the lifetime spectra and its value reflects how much defective a material is.

The average lifetime, τ_{av}, after irradiation at 600 °C increases by more than a factor of 2, denoting the creation of open volume defects in the lattice. As the irradiation temperature increases τ_{av} decreases indicating that at higher temperature the population of open volume defects decreases.

After irradiation, the PALS spectra are described by two lifetimes. The short lifetime, τ_1, has values in the range 130 to 176 ps and corresponds to annihilations in dislocations and in the defect-free part of the material (Fig. 4a). More specifically, after irradiation at 600 °C the short lifetime attains the value of (176±1) ps which decreases to (161±1) ps at the irradiation temperature of 800 °C. Further increase of the irradiation temperature to 900 °C does not significantly affect τ_1. However, after irradiation at 1200 °C τ_1 decreases to (130±1) ps. This decrease of τ_1 indicates the decrease of the dislocation density and the enhancement of positron annihilations in the defect-free part of the material.

The long lifetime, τ_2, has values in the range 512-534 ps (Fig. 4a) and it corresponds to annihilations in vacancy clusters having more than 40 vacancies and sizes larger than 1 nm. According to literature, voids having 13-37 vacancies have a lifetime of 410 - 440 ps [49], and a longest lifetime of 550 ps has been associated with large vacancy clusters containing more than 40 vacancies [9]. As the irradiation temperature increases from 600 to 900 °C the lifetime τ_2 increases linearly from 512 up to 534 ps, indicating the increase of the void size. Further increase of the irradiation temperature does not significantly affect the lifetime τ_2. It is noted that for large vacancy clusters (>40 vacancies) theoretical calculations predict a small or no

dependence of the positron lifetime on the void size due to the localization of positron at the cavity surface. Therefore, for large void sizes the lifetime τ_2 is insensitive to the size of the voids.

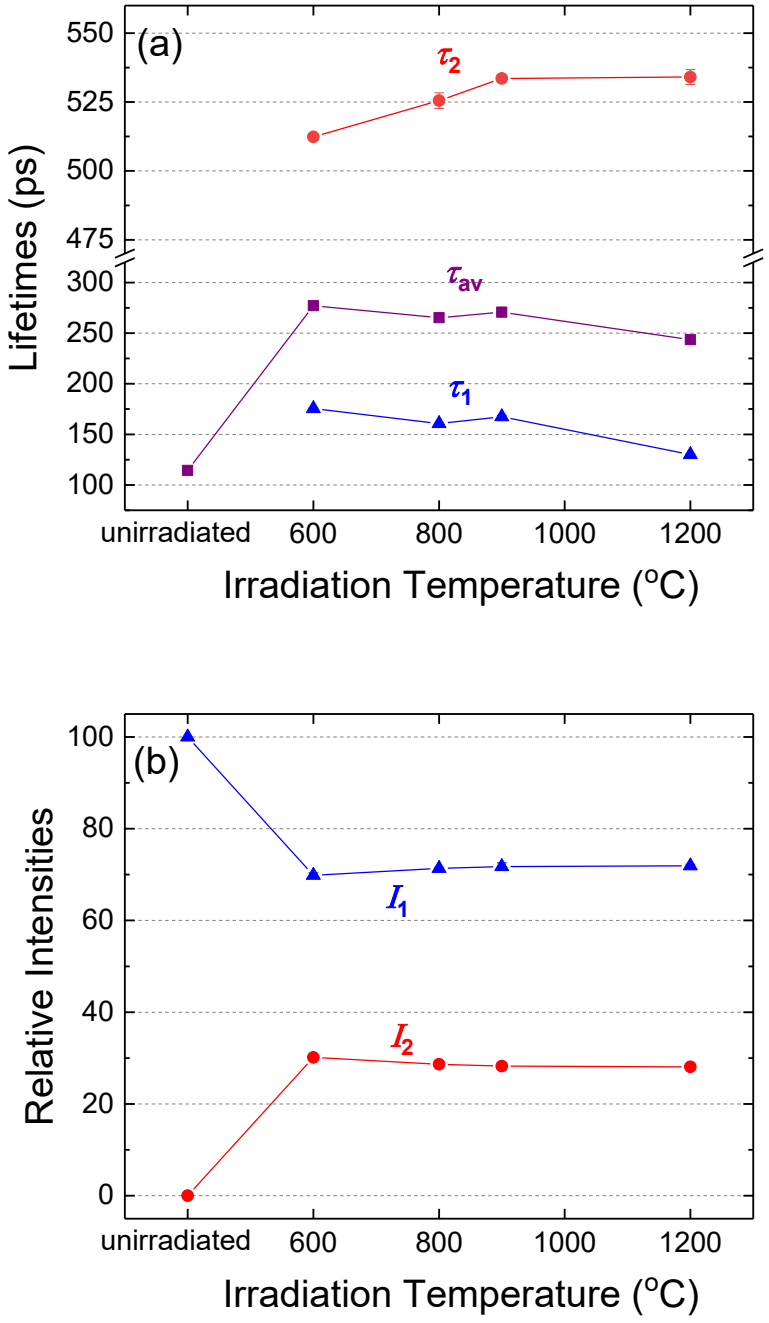

Fig. 4. (a) Positron lifetimes and (b) relative intensities for irradiated single crystal as a function of the irradiation temperature. The average lifetime τ_{av} for the unirradiated material corresponds to τ_0 (see Table 1).

The relative intensity of the long lifetime is almost constant at all irradiation temperatures having a value of about 29%. Since the intensity reflects the relative percentage of the positrons being annihilated at the various annihilation sites, it can be considered as a measure of the volume fraction of these sites. Thus, the constant intensity value, I_2, in combination with the increase of the void size as the irradiation temperature increase indicates the decrease of the number density of voids, most probably through the coalescence of small voids to larger ones.

Summarizing the above results, we conclude that irradiation at 600 °C results in the formation of dislocations as well as voids having a diameter of more than about 1 nm. As the irradiation temperature increases to 800 °C the coalescence of vacancy clusters to larger ones takes place. Further increase of the irradiation temperature to 900 °C does not significantly affect the volume fraction of the voids while neutron irradiation at 1200 °C results in a significant decrease of τ_1 reflecting the increase of positron annihilations in the defect-free bulk material and indicating the decrease of the total dislocations' density.

b) Forged bar

The lifetimes and their related intensities as determined by least squares fitting of eq. (2.1) to the PALS spectra are depicted in Fig. 5. Two lifetimes are needed to describe the PALS spectra.

At all irradiation temperatures an increase of the average positron lifetime, τ_{av}, is observed, compared to the unirradiated material, with its value ranging in the range from 303 to 372 ps indicating the creation of open volume defects in the lattice due to neutron irradiation. A maximum in the average lifetime is observed after irradiation at 800 °C implying that after irradiation at this temperature the material has the highest volume fraction of open volume defects.

As in the case of the SC material τ_1 is a weighted lifetime resulting from positron annihilations in dislocations and the bulk defect-free material. After irradiation in the temperature range 600 to 900°C τ_1 has a value of about (170 ± 2) ps. After irradiation at 1200 °C τ_1 decreases to the value of (154± 2) ps which is very close to the average lifetime of the unirradiated sample ((146 ± 7) ps). This decrease of τ_1 indicates the decrease in the dislocation density after irradiation at 1200 °C.

After irradiation at 600 °C a long lifetime, τ_2, is determined with a value of 498 ps (Fig. 5a). This lifetime corresponds to positron annihilations at large vacancy clusters or voids having more than 40 vacancies as discussed for the case of the single crystal material. The obtained values for τ_2 show that for all irradiation temperatures the voids have a diameter larger than

about 1 nm in agreement with TEM results [23]. Increase of the irradiation temperature results in the increase of τ_2. However, as already mentioned above, due to the localization of positron at the void's surface, the positron lifetime saturates and becomes insensitive to void size for large voids.

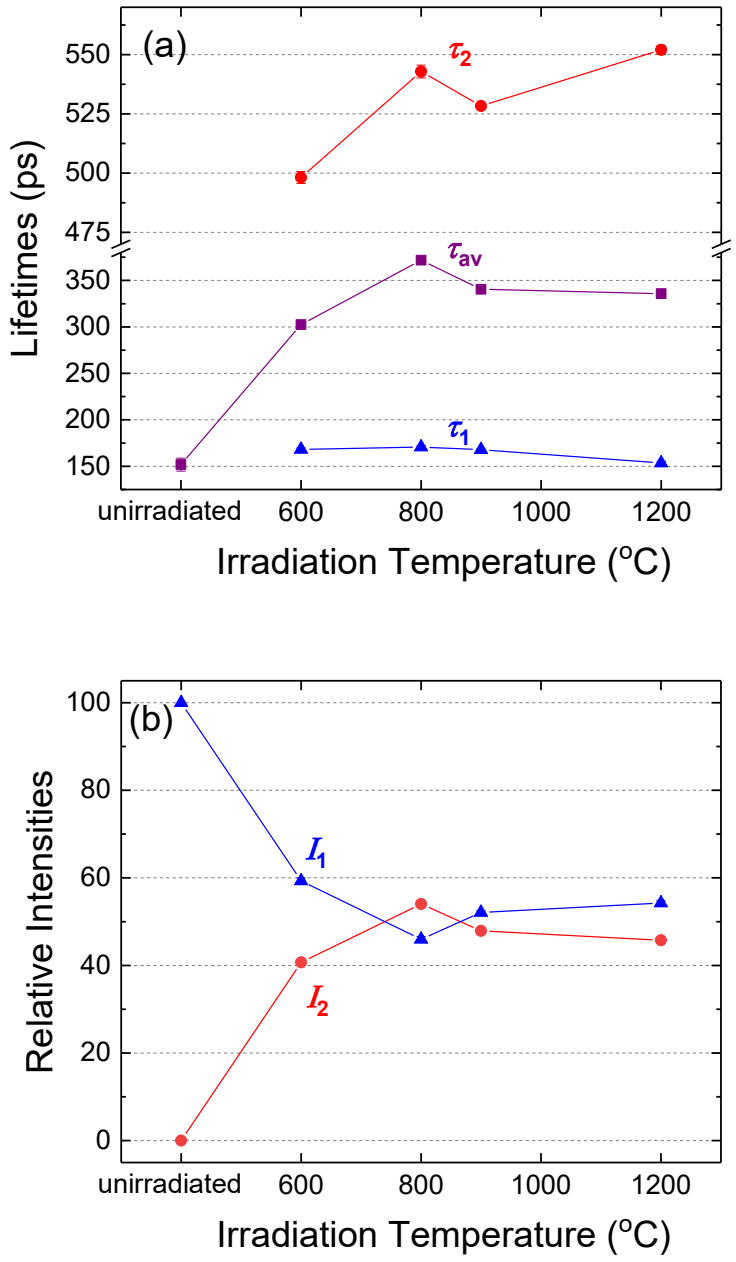

Figure 5. (a) Positron lifetimes and (b) relative intensities for irradiated forged bar as a function of the irradiation temperature. The average lifetime, τ_{av}, of the unirradiated material corresponds to τ_1 of the irradiated material (see Table 1).

The relative intensity, I_2, of the long lifetime increases from (41 ± 1)% after irradiation at 600 °C to I_2 = (54 ± 1) % after irradiation 800 °C. This increase in I_2 is probably caused by the increase of the trapping rate of the voids due to their size increase. Further increase of the irradiation temperature up to 1200 °C causes I_2 to decrease by about 15%, indicating a decrease in the number density of voids.

The picture that emerges about the evolution of the open volume defects in W forged bar is the following: irradiation at 600 °C results in the formation of dislocations and voids with the latter having a diameter of more than about 1 nm. As the irradiation temperature increases the void size increases reflecting the coalescence of small vacancy clusters to larger ones. The percentage of positrons being annihilated in voids presents a maximum at 800 °C, indicating a maximum in their volume fraction after irradiation at this temperature. Moreover, neutron irradiation at 1200 °C results in a decrease of τ_1, from (168 ± 1) ps after irradiation at 600 °C to (154 ± 2) ps, manifesting the increase of positron annihilations in the bulk material and indicating the decrease of the total dislocations' density.

c) <u>"Cold"-rolled sheet</u>

As in the case of SC and bar, two lifetimes are needed to describe the PALS spectra. The lifetimes and their related intensities are depicted in Fig. 6.

The average lifetime, τ_{av}, increases by a factor of two after irradiation at 600 °C and as the irradiation temperature increases further to 1200 °C τ_{av} presents a small linear increase, contrary to the behavior observed for W SC in which τ_{av} decreased with the increase of the irradiation temperature. This different behaviour of τ_{av} for W sheet suggests that the in-situ "healing" of the material due to the annealing as the irradiation temperature increases is not dominant.

After neutron irradiation at 600 °C, τ_1 increases from 160 ps for the unirradiated material to (184±1) ps. The obtained values of τ_1 correspond to a weighted average of positron annihilations in dislocations, in mono-vacancies (for which the reported positron lifetimes lie in the range 160-200 ps) and in the bulk defect free material. The increase of the irradiation temperature from 600 to 800 °C results in a small decrease of τ_1 to the value of (173±1) ps. Further increase of the irradiation temperature does not significantly change the value of τ_1. The observed decrease of τ_1 is attributed in the decrease of the dislocation density and the recovery of mono-vacancies either at dislocations or grain boundaries or through their coalescence to vacancy clusters.

After irradiation at 600 °C a long lifetime, τ_2, is found, having a value of (503 ± 4) ps, which corresponds, as in the case of the SC and the bar, to voids having more than 40 vacancies and a diameter larger than 1 nm. As the irradiation temperature increases to 1200 °C τ_2 continues to increase almost linearly to the value of (576 ± 2) ps, showing the growth of the voids in agreement with TEM results [23].

The relative intensity, I_2, of the long lifetime shows small variation as a function of the irradiation temperature, with values ranging between 45 and 51% and presenting a broad shallow maximum of (51 ± 1) % after irradiation at 900 °C.

Summarizing the above findings, we conclude that after irradiation at 600 °C dislocations, mono-vacancies and voids, with the latter having a size larger than about 1 nm, are formed. The mono-vacancies annihilate after irradiation at 800 °C. As the irradiation temperature increases, the void size increases, while the percentage of positrons being annihilated in voids presents a maximum at 900 °C, indicating a maximum in their volume fraction after irradiation at this temperature.

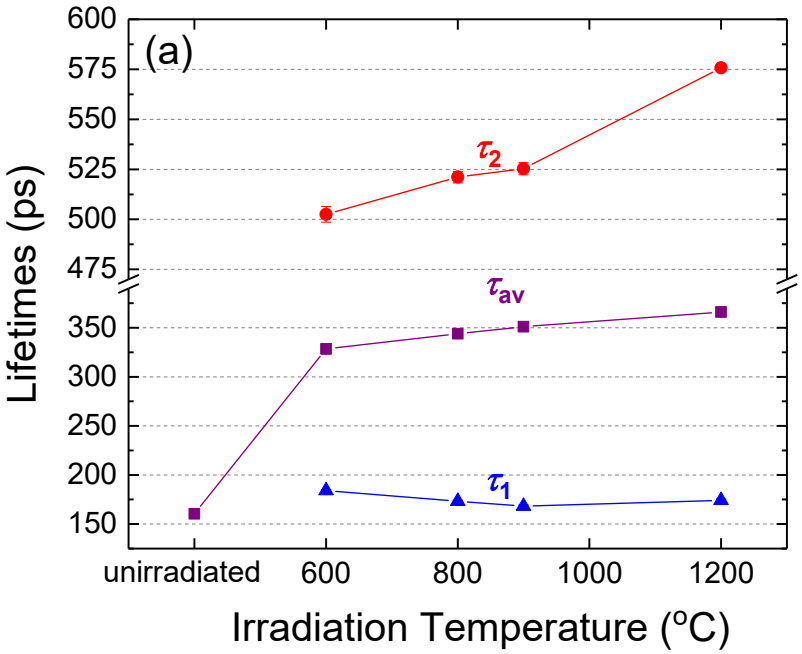

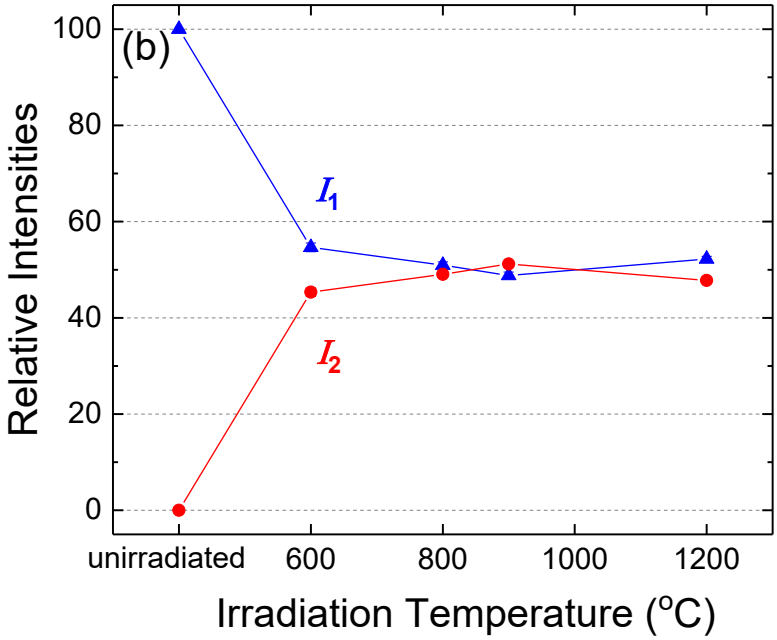

Figure 6. (a) Positron lifetimes and (b) relative intensities for irradiated "cold"-rolled sheet as a function of the irradiation temperature. The average lifetime, τ_{av}, of the unirradiated material corresponds to τ_1 of the irradiated material (see Table 1).

3.3 Trapping model results

The analysis above showed the existence of two distinct open volume defect groups, dislocations and voids, for all W materials and at all irradiation temperatures. Only for the "cold"-rolled sheet the short lifetime for the irradiation at 600 °C could involve a small percentage of positrons being annihilated at mono-vacancies. Therefore the two traps model could be used to obtain quantitative results for the defect densities.

The trapping model is described by the equation [55]

$$S(t) = B + R(t) \otimes \left(I_{src} + I_s \right) = B + R(t) \otimes \left(\sum_{k=1}^{L} I_k \lambda_k e^{-\lambda_k t} + I_0 \Lambda e^{-\Lambda t} + \sum_{i=1}^{N} I_i \lambda_i e^{-\lambda_i t} \right) \quad (2)$$

In the trapping model the intensities are related to the trapping rates, κ_i, through the equation

$$I_i = \frac{\kappa_i}{\Lambda - \lambda_i} \quad (3)$$

where $\Lambda = \lambda_0 + \sum_{i=1}^{2} \kappa_i$, $\lambda_0 = \tau_0^{-1}$ the inverse lifetime of the positron in the defect free material.

The trapping rate is related to the concentration, C_i, of the ith trap by

$$\kappa_i = \mu_i C_i \quad (4)$$

where μ_i the trapping strength of the ith trap. The trapping model can provide an estimation of the number density of each defect type (positron trap) in the irradiated tungsten as described below.

Below we discuss the application of the two-defect trapping model for the identified defects in the materials of the current study, namely voids and dislocations.

In the case of diffusion limited positron trapping in a spherical void of diameter d_{void} and number density N_{void} the positron trapping rate is described by the equation [56, 57]

$$\kappa_{void} = 2\pi d_{void} D_+ N_{void} \quad (5)$$

where D_+ the positron diffusion constant which can be determined from the equation [58]

$$L_+ = \sqrt{D_+ \tau} \quad (6)$$

where $L_+ = 135\ \mathrm{nm}$ the positron diffusion length in W [13] and τ the positron lifetime in the bulk defect-free W (~100 ps). Using eq. (5) the number density of voids can be determined using void diameter values from TEM literature data from the same W material and very similar irradiation dose [23].

The trapping rate for trapping in dislocations or cylindrical pores with radius r_d is given by [57]

$$\kappa_{disl} = \frac{4\pi D_+ N_{disl}}{\ln[1/(\pi N_{disl} r_d^2)]} \quad (7)$$

where N_{disl} the number density of dislocations. Using eq. (7) N_{disl} can be determined assuming r_d equals the magnitude of Burgers vector for W, $b = 0.274$ nm.

The two traps model presented above was used to analyze the PALS spectra. The positron lifetime in the defect free bulk tungsten was set to 100 ps and for the lifetime of the voids the values determined using eq. (1) and depicted in the Figs. 4, 5 and 6 were used, whereas for the positron lifetime for the dislocations was set to the value of 174 ps.

From the obtained trapping rates the void and dislocation densities have been calculated using eqs. (5) and (7) respectively. For the void sizes the values determined by TEM measurements on the same W materials irradiated to a similar dose of 0.18 dpa were used [23]. Since TEM measurements were not performed for $T_{irr} = 900\ ^{\circ}\mathrm{C}$ an interpolated value for the void size was calculated for this irradiation temperature.

In Fig. 7 the positron trapping rates for trapping in dislocations, κ_{disl}, are presented together with the corresponding dislocation density, N_{disl}, determined using eq. (7). It is observed that the dislocation density decreases as the irradiation temperature increases for all W types, presenting similar values for the different initial microstructures. In the temperature range from 800 to 900 °C no significant variation is observed. The obtained N_{disl} values are in satisfactory agreement with the dislocation density determined from TEM measurements of the same W types for a similar irradiation dose of 0.18 dpa [23].

In Fig. 8 the positron trapping rate at voids is depicted together with the corresponding void number density, N_{void}, obtained employing eq. (5). As the irradiation temperature increases the trapping rate and the void number density decrease. The comparison of N_{void} with that obtained by TEM measurements of the same W types irradiated to a similar dose of 0.18 dpa shows that the N_{void} values as determined by PALS are underestimated. The larger discrepancy is observed for the W SC and in general the higher the irradiation temperature the larger the percentage difference is. This can be understood with the following line of reasoning. As the irradiation temperature increases the average distance between voids increases and it becomes a significant fraction of the positron diffusion length (~135 nm) and therefore eq.(3) may no longer be valid [59]. In addition as the void size increases well beyond 1 nm the positron trapping at the surface of the void may no longer be described by Eq. (5) as discussed in [60] and references therein.

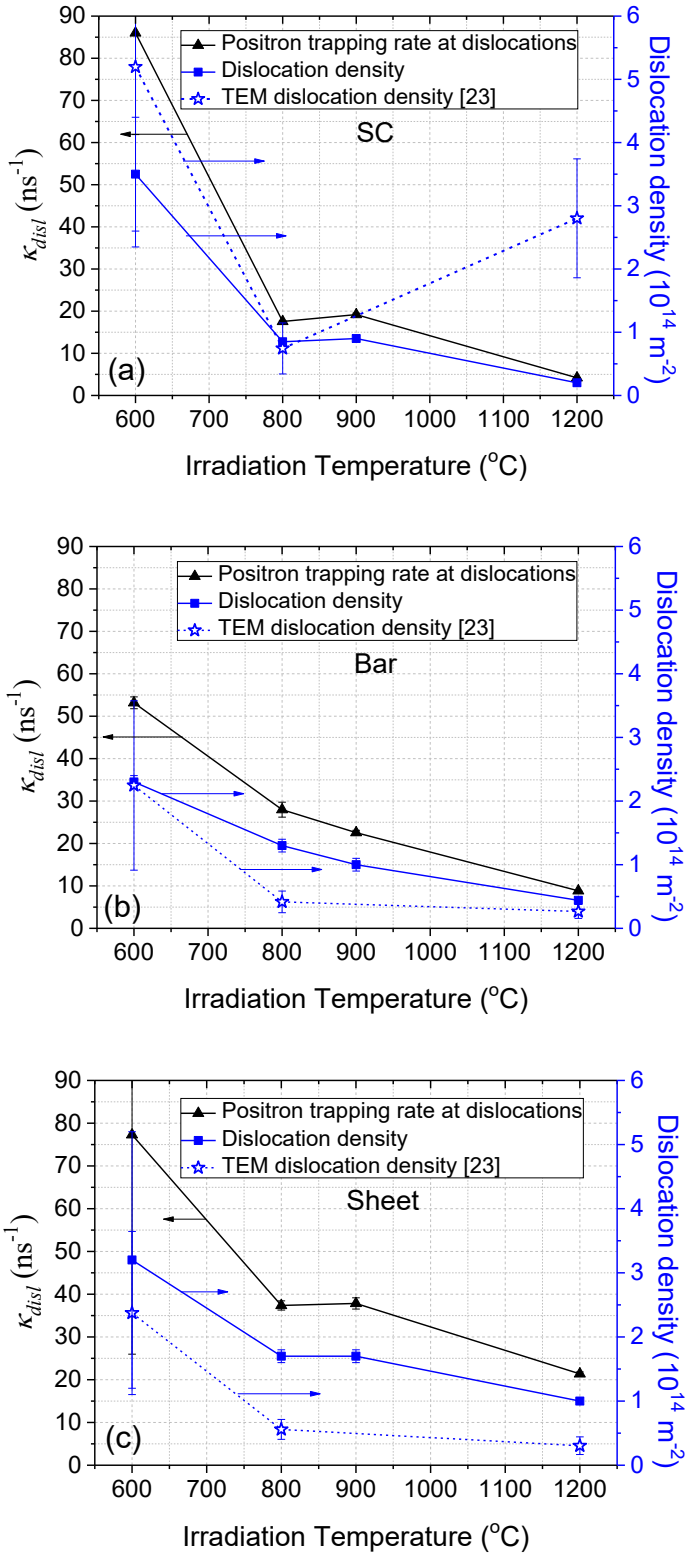

Figure 7. Positron trapping rates at dislocations and corresponding dislocation density according to eq. (7) for W SC (a), W bar (b) and W sheet (c). For comparison the dislocation density determined by TEM measurements according to [23] is presented.

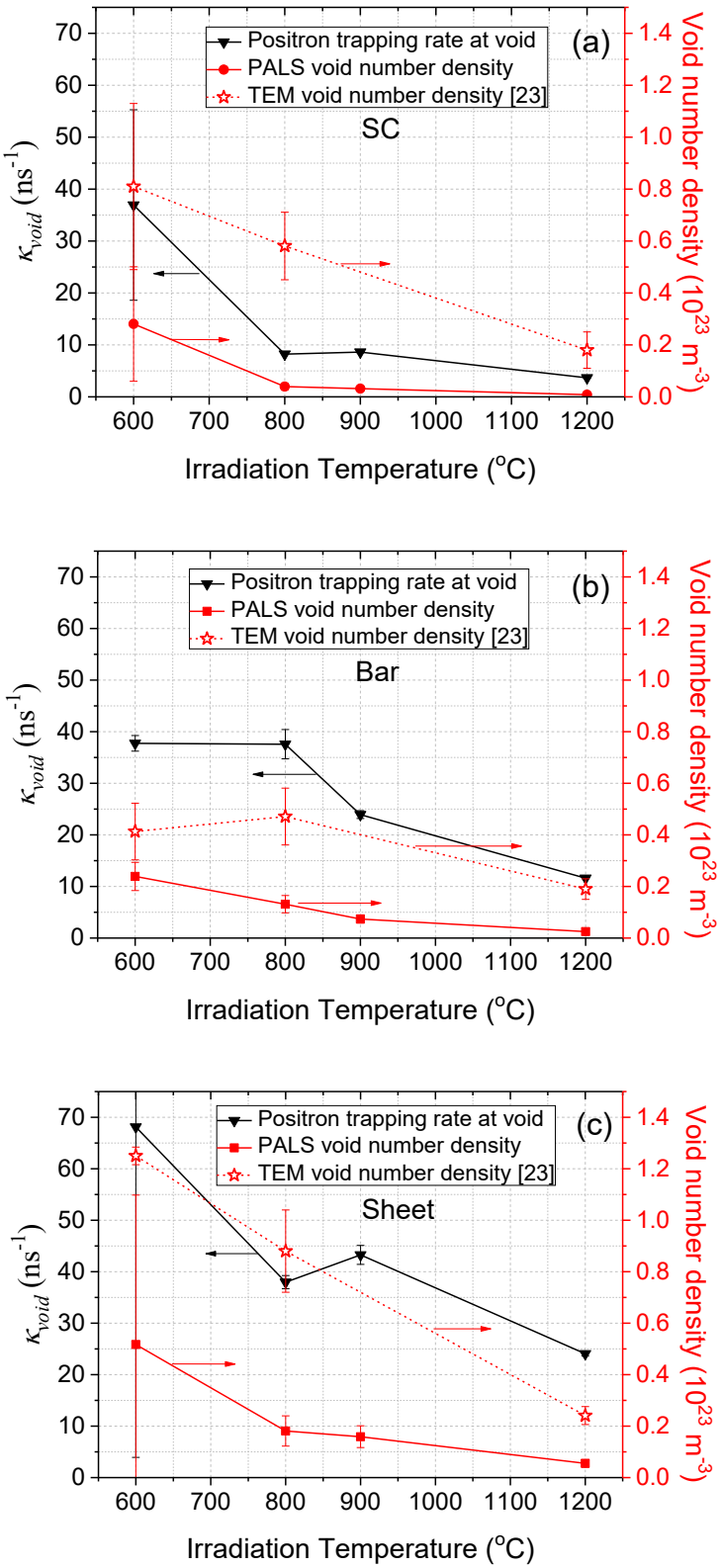

Figure 8. Positron trapping rates at voids and corresponding void number density according to eq. (5) for W SC (a), W bar (b) and W sheet (c). For comparison the void number density determined by TEM measurements according to [23] is presented.

3.4 Characterization of open volume defects using CDB-PAS

3.4.1 Unirradiated materials

The relative CDB spectra, n/n_{SC}, for the polycrystalline W grades, i.e., W bar and W sheet, with SC as reference are presented in Figure 9. As shown in the figure, the CDB spectra of both bar and sheet are very similar. Compared to SC, both W grades show a slight increase at the low momentum region, i.e., $p_L < 4\times10^{-3}\ m_0c$, followed by a larger increase in the region $(12\text{-}22)\times10^{-3}\ m_0c$. The increase in the low momentum region can be attributed to both the polycrystalline nature of the crystals and the significant dislocation density present in these grades. The increase in the higher momentum region could potentially be attributed to impurities present in the polycrystalline grades due to the industrial process (see for example Table 1 in [61] for typical levels of impurities in polycrystalline W grades) which have higher positron affinity than W [62]. However, this increase is subtle and it is not reflected in the S-W plot (see section 3.4.3). On the other hand, the statistical error in the high momentum region is large due to the limited statistics in the high momentum region compared to the low momentum region.

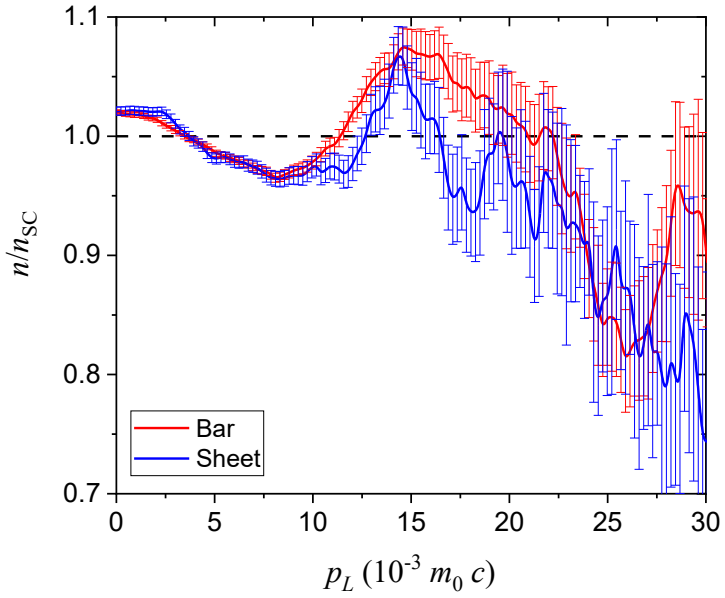

Figure 9. Relative CDB spectra, n / n_{SC}, for the W bar and W sheet compared to SC W. All curves were smoothed by moving average over 10 data points.

While a clear distinction can be observed between SC and the polycrystalline W grades, the differences between the W bar and W sheet are very subtle and probably better reflected by the S- and W-parameters (see Figure 12). A marginal increase for p_L < 4×10^{-3} m_0c and decrease for p_L in the range 12×10^{-3}-14×10^{-3} m_0c of the spectrum for the sheet compared to the bar is observed. The increase in the low momentum area for the sheet compared to the bar is consistent with the higher dislocation density observed in the former.

3.4.2 Irradiated materials

a) Single crystalline W(100)

In Figure 10, the relative CDB spectra, n_{irr} / n_{ref}, are presented for the different irradiation temperatures, where unirradiated SC W served as reference. In the temperature range 600-800 °C, there is a clear increase of the CDB spectra for low momenta, p_L<4×10^{-3} m_0c . For higher momenta, the CDB spectra reduce. The spectrum for the SC irradiated at 1200 °C is almost coincident with that of the unirradiated material. Thus, a clear effect of irradiation temperature is observed: the increase for low momenta reduces with the increase of the irradiation temperature and is almost fully recovered at 1200 °C.

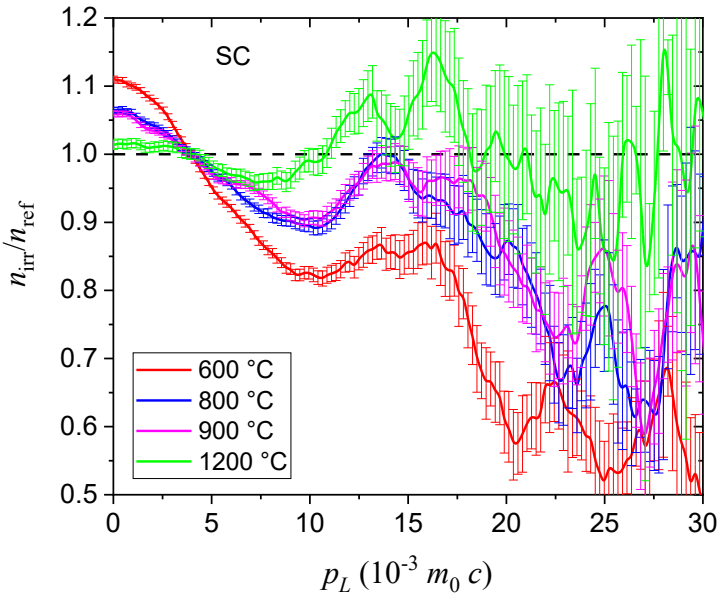

Figure 10. Relative CDB spectra, n_{irr} / n_{ref}, for the irradiated SC compared to unirradiated SC W. All curves were smoothed by moving average over 10 data points.

b) Polycrystalline W grades

In Figure 11, the relative CDB spectra, n_{irr} / n_{ref}, are presented for the different irradiation temperatures for the W bar and W sheet, respectively. As reference spectra the unirradiated W bar and W sheet were used, respectively. The obtained relative CDB spectra are almost identical for both grades. For all irradiation temperatures, a clear increase in the CDB spectrum is observed for low momenta, p_L<4×10^{-3} $m_0 c$, while for high momenta the spectra are reduced. The shape of the observed spectra is qualitatively very similar to the ones obtained for SC. However, unlike the case for SC, the irradiation temperature dependence of the CDB spectra is more subtle for the polycrystalline W grades and better reflected in the S- and W-parameters (see Figure 12).

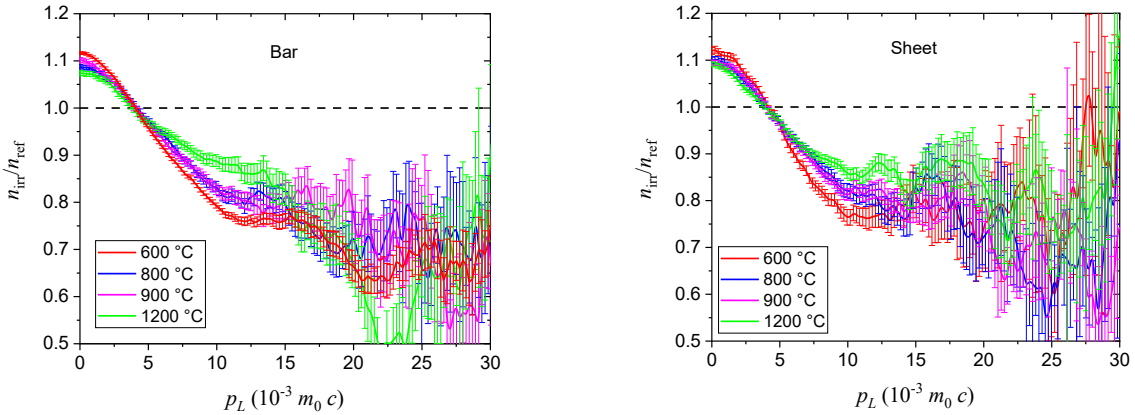

Figure 11. Relative CDB spectra, n_{irr} / n_{ref}, for the irradiated (left) W bar and (right) W sheet. As reference spectra, the unirradiated W bar and W sheet were used, respectively. All curves were smoothed by moving average over 10 data points.

3.4.3 S-W parameter analysis

The S-parameter reflects the population of the open volume defects, whereas the W-parameter depends on the chemical environment around the positron annihilation. Introduction of open volume defects results in the increase of the S- and the decrease of the W-parameter. The evolution of positron annihilation parameters is best monitored by the variation of S-W correlation plots. In such plots, different slopes in data sets can be correlated to different defect types. The S-W plot for our data is presented in Figure 12a. As already reported in [14], all data for SC lie on a straight line. Hereby the S- and W-parameter decreases/increases with irradiation temperature and almost fully recovers at 1200 °C to that of the unirradiated reference material which is an almost defect-free material as shown by the PALS measurements. The data for the polycrystalline W grades, i.e., both irradiated and unirradiated

samples, also follow the same straight line. This indicates that the open volume defect types (nano-voids and dislocations) introduced by the irradiation is the same in all W grades.

As discussed in depth in [14], the fact that all data follow the same straight line indicates that all damage is associated to the same type of open volume defects taking into account the fact that data obtained from plastically deformed and electron irradiated samples follow the same trend line (see [14]).

It is worth noting that the values for the S-parameter of the W bar are systematically lower than the values for the W sheet at the same irradiation temperature. This suggests that the irradiation damage recovers more efficiently in the bar compared to the sheet with irradiation temperature. This observation is consistent with the lower void density observed in the W bar compared to the W sheet (see Figure 8), especially at low irradiation temperature (also in the S-W plot the difference in the S- parameter between bar and sheet is the largest at the lowest irradiation temperature).

The CDB data obtained in the present work are compared to the data obtained by Hu et al. [9] in Figure 12b. In that work, single crystal W was neutron irradiated in the HFIR reactor at 90 °C up to 0.006 dpa and 0.03 dpa. After irradiation, the samples were post-irradiation annealed in the range 400-1300 °C. A non-negligible difference was observed in the absolute values of S- and W-parameters for reference SC W. Because the same limits were used for defining the S- and W-parameters, this difference is likely attributed to the use of different ^{22}Na sources which contribute to the CDB spectra. Therefore, each data set was normalized to the S- and W-parameters corresponding to reference SC W of the respective works. These are the values presented in Figure 12b.

Clearly, in Figure 12b all data falls on the same slope, indicating that the data sets generated in both works are consistent, i.e., the observed defect types are the same in both works. Further, the as-irradiated data in Hu et al. [9] is consistent with our SC data: the S-parameter for irradiation at 90 °C is larger than the one for irradiation at 600 °C, even though the accumulated dose is up to two orders of magnitude lower.

The data concerning post-irradiation annealing are extensively discussed in the work by Hu et al. [9] and will not be discussed here. The data was added with the sole purpose of showing that it fits the same slope as our data, and is thus consistent.

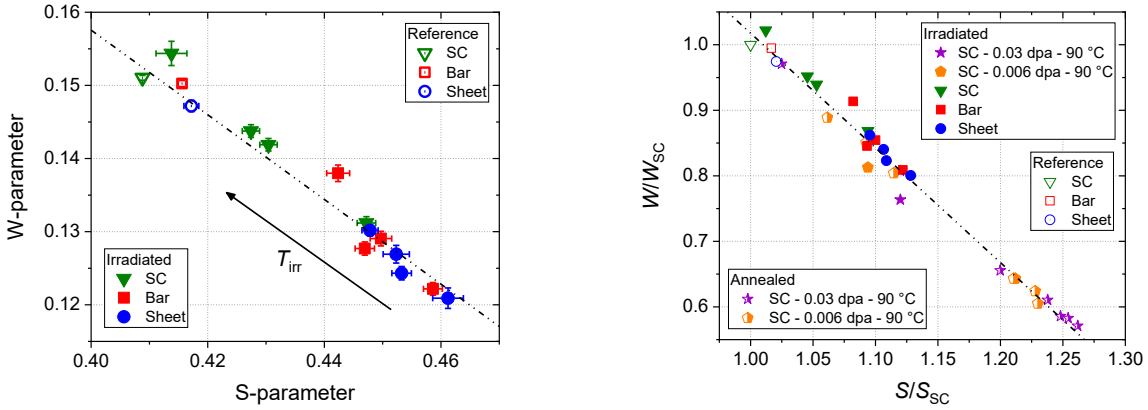

Figure 12. S-W plot of the data obtained from tungsten SC, bar and sheet (left) and the same plot using relative values for S-W enriched with data by Hu et al. [9] (right).

4 Discussion

In this section we compare the behavior of the three different W grades in order to investigate the effect of the initial microstructure in the neutron irradiation induced open volume defects.

The average positron lifetime, τ_{av}, for the three materials is presented in Figs. 4-6. τ_{av} is a measure of how defective the material is. The bar and sheet present similar τ_{av} values while the SC presents lower τ_{av} at almost all the irradiation conditions. Thus, it is inferred that the SC is systematically the less defective material for the same irradiation conditions. This is in agreement with the variation of the S parameter for the three W grades as depicted in Fig. 12. It is noted that the W polycrystalline grades have a considerable number of defects because of their fabrication process. The evolution of τ_{av} for the SC material as a function of the irradiation temperature shows damage recovery as the irradiation temperature increases and this becomes more apparent at the irradiation temperature of 1200 °C in line with the decrease of the S-parameter determined from the PAS-CDB measurements. For the bar a saturation of τ_{av} is observed after irradiation at 900 °C, whereas for the sheet material τ_{av} shows a small linear increase with the increase of the irradiation temperature.

After irradiation at 600 °C the short lifetime, τ_1, increases in the range 168 to 184 ps for all W materials (Fig. 13). Taking into account that τ_1 is a weighted average of annihilations in dislocations, possibly in mono-vacancies and to a much lesser degree in the defect free material, the higher value of τ_1 for the sheet in most of the irradiation conditions implies higher dislocation density and possibly higher density of mono-vacancies. The effect of the initial microstructure is more evident at the irradiation temperature of 1200 °C, with the sheet

presenting larger τ_1 value than that of the bar and SC. This implies a higher volume fraction of monovacancies for the sheet material trapped at the available sinks.

Regarding the long lifetime τ_2, which corresponds to positron annihilations in voids, similar values are observed for the three W types at all irradiation conditions (Fig. 13) leading to the conclusion that the voids are of similar size independent of the initial microstructure. However, as it is apparent in Fig. 13, τ_2 saturates after irradiation at 900 °C for the SC, while it keeps increasing from 900 to 1200 °C for the bar and sheet and this effect is more pronounced for the sheet than for the bar. This different evolution of τ_2 of the polycrystalline materials indicates that the initial microstructure affects the accumulation and growth of voids. Moreover, it might be inferred that in the temperature range 800 – 900 °C the initial microstructure of the polycrystalline materials suppresses the void growth thanks to sinking at available dislocations and grain boundaries.

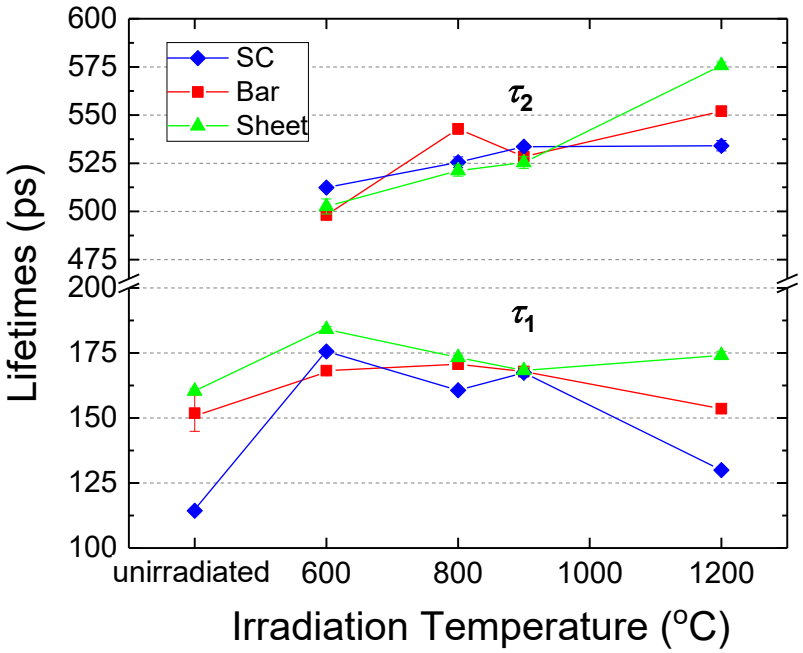

Figure 13. Positron lifetimes for all W grades.

After irradiation at 600 °C the intensity of the long positron lifetime, I_2, is significantly larger for the sheet (45%) and the bar (41%) than that of the SC (30%) which indicates that the voids volume fraction that affects positron annihilation at these sites increases with the increase of the dislocations pre-existing in the unirradiated material due to the fabrication

process. After irradiation at 800 °C or 900 °C I_2 presents a shallow maximum for the bar and the sheet, respectively, and very similar values which decrease likewise as the irradiation temperature increases. On the contrary, for the SC I_2 is slightly reduced to about 28% after irradiation at 800 °C and saturates for higher irradiation temperatures. The difference in the values of I_2 between the polycrystalline materials and the SC reflect the influence of the initial microstructure (grain boundaries and dislocations) in the void growth and this difference becomes more apparent after irradiation at 1200 °C. Thus, it may be inferred that the plastic deformation of the polycrystalline W suppresses void dissolution and this is probably related to the stress field in the material. This is further confirmed by the larger void size found for the W sheet. In addition, this inference is in agreement with the void size distribution observed in TEM measurements of the same W materials irradiated to a similar dose of 0.18 dpa, in which no voids with diameter larger than 2 nm are observed in the SC contrary to those observed in the heavily deformed sheet [23]. Moreover, corroboration for this is provided by the fact that the higher stress field increases the long-range attractive force between the interstitials and the dislocations allowing an excessive vacancy flux at the voids [63]. Also the higher percentage of impurities in the W polycrystalline materials may pay role to this effect as it is known that impurities can act as stabilization sites for vacancy clusters [63].

The results from the PAS-CDB are fully consistent with the presented PALS data. In particular, it must be noted that reduction of the S-parameter and even recovery of the S-parameter does not necessarily mean that all damage is recovered. As explained in [14] for SC, the reduction and recovery of the S parameter with irradiation temperature correspond to the growth and saturation of void size and the reduction or saturation of their density. The latter is indeed observed in Fig. 2, i.e. the long lifetime increases and saturates with the increase of the irradiation temperature, while its intensity saturates or slightly decreases with temperature. For the polycrystalline W grades, the same reasoning can be applied: the long lifetime increases with irradiation temperature while its intensity saturates.

The application of the two-defect trapping model, with the one defect group being the dislocations and the other the voids, enables the determination of the density for the two defect types. It is found that the dislocation density decreases as the irradiation temperature increases and the obtained values are comparable to the values obtained by TEM for a similar but slightly higher neutron irradiation dose of 0.18 dpa. Regarding the void density, it is found to decrease with irradiation temperature, with a decreasing ~~decrease~~ rate as the irradiation temperature increases. The determined density for the voids is much lower than that obtained by TEM measurements, which indicates that the trapping process as described by eq. (5) is not adequate to describe positron annihilation at voids and more elaborate trapping processes as the diffusion-reaction-controlled trapping modeling might be more appropriate [60].

5 Summary and conclusions

Two polycrystalline W grades, having different degree of plastic deformation, i.e. ITER grade forged bar and heavily deformed “cold”-rolled sheet, and a single crystal W(100) were neutron irradiated in the temperature range between 600 and 1200 °C at the Belgian Material Test Reactor (BR2) to a fast neutron fluence of 5.8×10^{20} n/cm^2, (E>0.1 MeV) corresponding to a dose of 0.12 dpa. Positron annihilation lifetime (PALS) and coincidence Doppler broadening (PAS-CDB) spectroscopy has been applied to study the evolution of open volume defects as a function of the irradiation temperature. From the analysis of the PALS spectra two positron lifetimes were identified at all irradiation temperatures and for all W grades, a short lifetime that corresponds to dislocations and possibly mono-vacancies, and a long lifetime characteristic of voids having sizes more than about 1 nm. From the PAS-CDB results it is confirmed that all damage is associated to the same type of open volume defects. The two traps model was employed to quantify the defect densities. The number density of both the dislocations and voids decreases as the irradiation temperature increases, with decreasing rate as the irradiation temperature increases. Moreover, the void size increases with the increase of the irradiation temperature. It is found that the plastic deformation of the polycrystalline W bar and sheet in combination with a higher percentage of impurities suppress the dissolution of the voids.

Acknowledgments

This work has been carried out within the framework of the EUROfusion Consortium and has received funding from the Euratom research and training programme 2014-2018 and 2019-2020 under Grant Agreements No. 633053. The views and opinions expressed herein do not necessarily reflect those of the European Commission. Also is acknowledged the support of the programme “NCSRD – INRASTES research activities in the framework of the national RIS3" (MIS 5002559) which is implemented under the “Action for the Strategic Development on the Research and Technological Sector”, funded by the Operational Programme "Competitiveness, Entrepreneurship and Innovation" (NSRF 2014-2020) and co-financed by Greece and the European Union (European Regional Development Fund). The funding from the Greek National Programme for the Controlled Thermonuclear Fusion is acknowledged.
We thank Dr Michael Rieth from Karlsruhe Institute of Technology, Germany, and Dr Gerald Pintsuk from Forschungszentrum Jülich GmbH, Germany, for the supply of the tungsten “cold”-rolled sheet and forged bar material, respectively.

References

[1] G. Pintsuk. Tungsten as a plasma-facing material. In Comprehensive Nuclear Materials (Vol. 4) (2012). Elsevier Inc. https://doi.org/10.1016/B978-0-08-056033-5.00118-X

[2] S. Wurster, N. Baluc, M. Battabyal, T. Crosby, J. Du, C. García-Rosales, A. Hasegawa, A. Hoffmann, A. Kimura, H. Kurishita, R.J. Kurtz, H. Li, S. Noh, J. Reiser, J. Riesch, M. Rieth, W. Setyawan, M. Walter, J.H. You, and R. Pippan, Recent progress in R&D on tungsten alloys for divertor structural and plasma facing materials. Journal of Nuclear Materials 442(1-3 SUPPL.1) (2013) 181–189. https://doi.org/10.1016/j.jnucmat.2013.02.074

[3] M. Rieth, R. Doerner, A. Hasegawa, Y. Ueda, and M. Wirtz. Behavior of tungsten under irradiation and plasma interaction. Journal of Nuclear Materials 519 (2019) 334–368. https://doi.org/10.1016/j.jnucmat.2019.03.035

[4] http://www.euro-fusion.org/

[5] A. Hasegawa, T. Tanno, S. Nogami, and M. Satou, Property change mechanism in tungsten under neutron irradiation in various reactors. Journal of Nuclear Materials, 417(1–3) (2011) 491–494. https://doi.org/10.1016/j.jnucmat.2010.12.114

[6] A. Hasegawa, M. Fukuda, T. Tanno, S. Nogami, Neutron irradiation behavior of tungsten. Materials Transactions 54(4) (2013) 466–471. https://doi.org/10.2320/matertrans.MG201208

[7] A. Hasegawa, M. Fukuda, S. Nogami, and K. Yabuuchi, Neutron irradiation effects on tungsten materials. Fusion Engineering and Design 89(7–8) (2014) 1568–1572. https://doi.org/10.1016/j.fusengdes.2014.04.035

[8] A. Hasegawa, M. Fukuda, K. Yabuuchi, S. Nogami, Neutron irradiation effects on the microstructural development of tungsten and tungsten alloys. Journal of Nuclear Materials 471 (2016) 175–183. https://doi.org/10.1016/j.jnucmat.2015.10.047

[9] X. Hu, T., Koyanagi, M. Fukuda, Y. Katoh, L.L. Snead and B.D. Wirth, Defect evolution in single crystalline tungsten following low temperature and low dose neutron irradiation. Journal of Nuclear Materials 470 (2016) 278–289. https://doi.org/10.1016/j.jnucmat.2015.12.040

[10] X. Hu, T. Koyanagi, M. Fukuda, N. A. P. K. Kumar, L. L. Snead, B. D. Wirth and Y.Katoh, Irradiation hardening of pure tungsten exposed to neutron irradiation. Journal of Nuclear Materials 480 (2016) 235–243. https://doi.org/10.1016/j.jnucmat.2016.08.024

[11] M. Fukuda, N. A. P. Kiran Kumar, T. Koyanagi, L.M. Garrison, L.L. Snead, Y. Katoh,and A. Hasegawa, Neutron energy spectrum influence on irradiation hardening and microstructural development of tungsten. Journal of Nuclear Materials 479 (2016) 249–254. https://doi.org/10.1016/j.jnucmat.2016.06.051

[12]T.Koyanagi, N. A. P. K. Kumar, T. Hwang, L. M. Garrison, X. Hu, L. L. Snead and Y.Katoh, Microstructural evolution of pure tungsten neutron irradiated with a mixed energy spectrum. Journal of Nuclear Materials 490 (2017) 66–74. https://doi.org/10.1016/j.jnucmat.2017.04.010

[13] L. M.Garrison, Y. Katoh and N. A. P. K. Kumar, Mechanical properties of single-crystal tungsten irradiated in a mixed spectrum fission reactor. Journal of Nuclear Materials 518 (2019) 208–225. https://doi.org/10.1016/j.jnucmat.2019.02.050

[14] G. Bonny, M.I. Konstantinovic, A. Bakaeva, Y. Chao, N. Castin, K. Mergia, V. Chatzikos, S. Dellis, T. Khvan, A. Bakaev, A. Dubinko and D. Terentyev, Trends in vacancy distribution and hardness of high temperature neutron irradiated single crystal tungsten. Acta Materialia 198 (2020). 1–9. https://doi.org/10.1016/j.actamat.2020.07.047

[15] R. K. Williams, F. W. Wiffen, J.Bentley and J. O. Stiegler, Irradiation induced precipitation in tungsten based, W-Re alloys. Metallurgical Transactions. A, Physical Metallurgy and Materials Science 14 A(4) (1983) 655–666. https://doi.org/10.1007/BF02643781

[16] Y. Nemoto, A. Hasegawa, M. Satou, K. Abe, Microstructural development of neutron irradiated W-Re alloys. Journal of Nuclear Materials 283–287(PART II) (2000) 1144–1147. https://doi.org/10.1016/S0022-3115(00)00290-7
[17] M. Fukuda, A. Hasegawa, T. Tanno, S. Nogami, H. Kurishita, Property change of advanced tungsten alloys due to neutron irradiation. Journal of Nuclear Materials 442(1-3 SUPPL.1) (2013) S273–S276. https://doi.org/10.1016/j.jnucmat.2013.03.058
[18] M. Fukuda, K. Yabuuchi, S. Nogami, A. Hasegawa, T. Tanaka, Microstructural development of tungsten and tungsten-rhenium alloys due to neutron irradiation in HFIR. Journal of Nuclear Materials 455(1–3) (2014) 460–463. https://doi.org/10.1016/j.jnucmat.2014.08.002
[19] J. C. He, G. Y. Tang, A. Hasegawa and K. Abe, Microstructural development and irradiation hardening of W and W-(3-26) wt%Re alloys after high-temperature neutron irradiation to 0.15 dpa. Nuclear Fusion 46(11) (2006) 877–883. https://doi.org/10.1088/0029-5515/46/11/001
[20] S. Das, Recent advances in characterising irradiation damage in tungsten for fusion power. SN Applied Sciences 1(12) (2019) 1–20. https://doi.org/10.1007/s42452-019-1591-0
[21] M. Dürrschnabel, M. Klimenkov, U. Jäntsch, M. Rieth, H.C. Schneider, & D. Terentyev, New insights into microstructure of neutron - irradiated tungsten, Nature Scientific Reports (2021) 1–17. https://doi.org/10.1038/s41598-021-86746-6
[22] S. Dellis, X. Xiao, D. Terentyev, K. Mergia, S. Krimpalis, A. Bakaev, S. Messoloras, Mechanical properties of neutron-irradiated single crystal tungsten W(100) studied by indentation and FEM modelling, J. Nucl. Mater. (2021) 152985. https://doi.org/10.1016/j.jnucmat.2021.152985
[23] A. Dubinko , D. Terentyev, C.Yin, W. Van Renterghem, B. Rossaert, M. Rieth, E. E. Zhurkin, A. Zinovev, C.-C. Chang, S. Van Dyck, & G. Bonny, Microstructure and hardening induced by neutron irradiation in single crystal, ITER specification and cold rolled tungsten. International Journal of Refractory Metals and Hard Materials 98 (2021) 105522. https://doi.org/10.1016/j.ijrmhm.2021.105522
[24] K. Mergia, V. Chatzikos, E. Manios, S. Dellis, D. Papadakis, D. Terentyev, G. Bonny, A. Dubinko, I.E. Stamatelatos, S. Messoloras and M. Rieth, "Evolution of microstructure in neutron irradiated cold rolled tungsten and its correlation with hardness", Fusion Eng. Des. 172 (2021) 112784. https://doi.org/10.1016/j.fusengdes.2021.112784
[25] D. Papadakis, S. Dellis, V. Chatzikos, E. Manios, I.E. Stamatelatos, S. Messoloras and K. Mergia, Neutron irradiation effects in different tungsten microstructures, 96 (2021) 124041. https://doi.org/10.1088/1402-4896/ac1eb2
[26] D. Papadakis, S. Dellis, K. Mergia, V. Chatzikos, D. Terentyev, G. Bonny, A. Dubinko, W. Van Renterghem, M. Konstantinovic, S. Messoloras and G. Pintsuk, The competing effects of temperature and neutron irradiation on the microstructure and mechanical properties of ITER grade tungsten, Fusion Engineering and Design 168 (2021) 112608. https://doi.org/10.1016/j.fusengdes.2021.112608
[27] C. Yin, G. Bonny, D. Terentyev, Anisotropy in the hardness of single crystal tungsten before and after neutron irradiation, J. Nucl. Mater. 546 (2021) 152759. https://doi.org/10.1016/j.jnucmat.2020.152759.
[28] V. K. Sikka, J. Moteff, Superlattice of voids in neutron-irradiated tungsten. Journal of Applied Physics 43 (2013) 4942. https://doi.org/10.1063/1.1661050.
[29] S. Bonk, J. Reiser, J. Hoffmann, and A. Hoffmann, Cold rolled tungsten (W) plates and foils: Evolution of the microstructure. International Journal of Refractory Metals and Hard Materials 60 (2016) 92–98. https://doi.org/10.1016/j.ijrmhm.2016.06.020
[30] M. Wirtz, I. Uytdenhouwen, V. Barabash, F. Escourbiac, T. Hirai, J. Linke, T. Loewenhoff, S. Panayotis, G. Pintsuk, Material properties and their influence on the behaviour of tungsten as plasma facing material, Nucl. Fusion. 57 (2017). https://doi.org/10.1088/1741-4326/aa6938.

[31] S. Krimpalis, K. Mergia, S. Messoloras, A. Dubinko, D. Terentyev, K. Triantou, J. Reiser, G. Pintsuk, Comparative study of the mechanical properties of different tungsten materials for fusion applications, Phys. Scr. 2017 (2017). https://doi.org/10.1088/1402-4896/aa9292.
[32] D. Pelowitz, J. Durkee, J. Elson, M. Fensin, R. Johns, G. McKinney, S. Mashnik, J. Verbeke, L. Waters, T. Wilcox, MCNPX 2.7.0 Extensions, 2011
[33] M.J. Norgett, M.T. Robinson, I.M. Torrens, A proposed method of calculating displacement dose rates, Nucl. Eng. Des. 33 (1975) 50–54. doi:10.1016/0029-5493(75)90035-7.
[34] Positrons in Solids, Editor: P. Hautojarvi in Topics in Current Physics, Vol. 12, Springer-Verlag Berlin Heidelberg New York 1979
[35] M. Eldrup and B. N. Singh, Studies of defects and defect agglomerates by positron annihilation spectroscopy. Journal of Nuclear Materials 251 (1997) 132–138. https://doi.org/10.1016/S0022-3115(97)00221-3
[36] D. Giebel, J. Kansy, LT10 program for solving basic problems connected with defect detection, Physics Procedia 35 (2012) (Positron Studies of defects 2011), pp. 122-127
[37] D. Giebel, J. Kansy, A new version of LT program for positron lifetime spectra analysis, Materials Science Forum (2011), pp. 138-141
[38] G. Dlubek, A. Sen Gupta, J. Pionteck, R. Häßler, R. Krause-Rehberg, H. Kaspar, K.H. Lochhaas, "Glass transition and free volume in the mobile (MAF) and rigid (RAF) amprphous fractions of semicrystalline PTFE: a positron lifetime and PVT study", Polymer 46 (2005), pp. 6075-6089
[39]O. V. Ogorodnikova, M. Majerle, V. V. Gann, J. Čížek, P. Hruška, S. Simakov, M. Štefánik and V. Zach, Verification of the theory of primary radiation damage by comparison with experimental data. Journal of Nuclear Materials 525 (2019) 22–31. https://doi.org/10.1016/j.jnucmat.2019.07.019
[40] G.S. Kanda, L. Ravelli, B. Löwe, W. Egger, D.J. Keeble, Positron Annihilation lifetime spectroscopy study of Kapton thin foils, Journal of Physics D: Applied Physics, 49 (2016) 025305
[41] J. Kansy, Kmroczka, J. Dutkiewicz, PALS determination of defect density within friction stir welded joints of aluminium alloys, Journal of Physics: Conference Series 265 (2011) 012010
[42] J. Kansy, A. Hanc-Kuczkowska, D. Giebel, Change of the defect structure in FeAl alloy as a result of its aging at ambient temperature, Nukleonika 58(1) (2013) pp. 221-224
[43] M.J. Konstantinović, G. Bonny, Thermal stability and the structure of vacancy-solute clusters in iron alloys, Acta Mater. 85 (2015) 107–111. https://doi.org/10.1016/j.actamat.2014.11.026.
[44] M.J. Konstantinović, I. Uytdenhouwen, G. Bonny, N. Castin, L. Malerba, P. Efsing, Radiation induced solute clustering in high-Ni reactor pressure vessel steel, Acta Mater. 179 (2019) 183–189. https://doi.org/10.1016/j.actamat.2019.08.028.
[45] J.M. Campillo Robles, F. Plazaola, Collection of data on positron lifetimes and vacancy formation energies of the elements of the periodic table, Defect Diffus. Forum. 213–215 (2003) 141–236. https://doi.org/10.4028/www.scientific.net/ddf.213-215.141.
[46] M.J. Puska, Ab-initio calculation of positron annihilation rates in solids, J. Phys. Condens. Matter. 3 (1991) 3455–3469. https://doi.org/10.1088/0953-8984/3/20/007.
[47] T.E.M. Staab, R. Krause-Rehberg, B. Vetter, B. Kieback, The influence of microstructure on the sintering process in crystalline metal powders investigated by positron lifetime spectroscopy: I. Electrolytic and spherical copper powders, J. Phys. Condens. Matter. 11 (1999) 1757–1786. https://doi.org/10.1088/0953-8984/11/7/009.
[48] S. Zhu, Y. Xu, Z. Wang, Y. Zheng, D. Zhou, E. Du, D. Yuan, M. Fukuda, M. Mihara, K. Matsuta, T. Minamisono, Positron annihilation lifetime spectroscopy on heavy ion irradiated stainless steels and tungsten, J. Nucl. Mater. 343 (2005) 330–332. https://doi.org/10.1016/j.jnucmat.2004.11.024.
[49] T. Troev, E. Popov, N. Nankov, T. Yoshiie, Model calculation of positron states in tungsten containing hydrogen and helium, J. Phys. Conf. Ser. 207 (2010). https://doi.org/10.1088/1742-6596/207/1/012033.

[50] P. Staikov, N. Djourelov, Simulations of 〈1 0 0〉 edge and 1/2〈1 1 1〉 screw dislocations in α-iron and tungsten and positron lifetime calculations, Phys. B Condens. Matter. 413 (2013) 59–63. https://doi.org/10.1016/j.physb.2012.12.026.
[51] J. Heikinheimo, K. Mizohata, J. Räisänen, T. Ahlgren, P. Jalkanen, A. Lahtinen, N. Catarino, E. Alves, F. Tuomisto, Direct observation of mono-vacancy and self-interstitial recovery in tungsten, APL Mater. 7 (2019). https://doi.org/10.1063/1.5082150.
[52] O. V. Ogorodnikova, M. Majerle, V. V. Gann, J. Čížek, P. Hruška, S. Simakov, M. Štefánik, V. Zach, Verification of the theory of primary radiation damage by comparison with experimental data, J. Nucl. Mater. 525 (2019) 22–31. https://doi.org/10.1016/j.jnucmat.2019.07.019
[53] P.E. Lhuillier, M.F. Barthe, P. Desgardin, W. Egger, P. Sperr, Positron annihilation studies on the nature and thermal behaviour of irradiation induced defects in tungsten, Phys. Status Solidi. 6 (2009) 2329–2332. https://doi.org/10.1002/pssc.200982114
[54] A. Yabuuchi, M. Tanaka, & A. Kinomura. (2020). Short positron lifetime at vacancies observed in electron-irradiated tungsten: Experiments and first-principles calculations. Journal of Nuclear Materials, 542. https://doi.org/10.1016/j.jnucmat.2020.152473
[55] A. Seeger, The study of defects in crystals by positron annihilation, Appl. Phys. 4 (1974) 183–199. https://doi.org/10.1007/BF00884229
[56] J. Pang, H. Li, K. Zhou, Z. Wang, The Correlation Between Dislocations and Vacancy Defects Using Positron Annihilation Spectroscopy, Plasma Sci. Technol. 14 (2012) 650–655. https://doi.org/10.1088/1009-0630/14/7/19
[57] W. Brandt, R. Paulin, Positron Diffusion in Solids, Phys. Rev. B. 5 (1972) 2430–2435. https://doi.org/10.1103/PhysRevB.5.2430
[58] A. Vehanen, K.G. Lynn, P.J. Schultz, M. Eldrup, Improved slow-positron yield using a single crystal tungsten moderator, Appl. Phys. A Solids Surfaces. 32 (1983) 163–167. https://doi.org/10.1007/BF00616613
[59] W.E. Frieze, K. G. Lynn and D.O. Welch, "Positron trapping," Phys. Rev. B vol. 31 (1985) 31. https://doi.org/10.1103/PhysRevB.31.15
[60] R. Würschum, L. Resch, and G. Klinser, "Diffusion-reaction model for positron trapping and annihilation at spherical extended defects and in precipitate-matrix composites," PHYSICAL REVIEW B 97 224108 (2018) pp. 1–11, https://doi.org/10.1103/PhysRevB.97.224108
[61] N. Castin, A. Bakaev, D. Terentyev, M. I. Pascuet, and G. Bonny, "Understanding why dislocation loops are visible in transmission electron microscopy : The tungsten case," J. Nucl. Mater., vol. 555, p. 153122, 2021, doi: 10.1016/j.jnucmat.2021.153122.
[62] M. J. Puska, P. Lanki, and R. M. Nieminen, "Positron affinities for elemental metals," J. Phys. Condens. Matter, vol. 1 (1989) 6081–6094, doi: 10.1088/0953-8984/1/35/008.
[63] V. F. Sears, "Kinetics of void growth in irradiated metals," Journal of Nuclear Material. 39 (1971) 1447-1451. https://doi.org/10.1016/0022-3115(71)90179-6